

1 **A first intercomparison of the simulated LGM carbon**
2 **results within PMIP-carbon: role of the ocean**
3 **boundary conditions**

4 **F. Lhardy¹, N. Bouttes¹, D. M. Roche^{1,2}, A. Abe-Ouchi³, Z. Chase⁴, K. A.**
5 **Crichton⁵, R. Ivanovic⁶, M. Jochum⁷, M. Kageyama¹, H. Kobayashi³, L.**
6 **Menviel⁸, J. Muglia⁹, R. Nuterman⁷, A. Oka³, G. Vettoretti⁷, A. Yamamoto¹⁰**

7 ¹Laboratoire des Sciences du Climat et de l'Environnement, CEA-CNRS-UVSQ, Gif-sur-Yvette, France

8 ²Vrije Universiteit Amsterdam, Faculty of Science, Department of Earth Sciences, Earth and Climate
9 cluster, Amsterdam, The Netherlands

10 ³Atmosphere and Ocean Research Institute, The University of Tokyo, Kashiwa, Japan

11 ⁴University of Tasmania, Hobart, Australia

12 ⁵School of Geography, Exeter University, Exeter, UK

13 ⁶University of Leeds, Leeds, UK

14 ⁷Niels Bohr Institute, University of Copenhagen, Copenhagen, Denmark

15 ⁸Climate Change Research Centre, the University of New South Wales, Sydney, Australia

16 ⁹Centro para el Estudio de los Sistemas Marinos, CONICET, 2915 Boulevard Brown, U9120ACD, Puerto
17 Madryn, Argentina

18 ¹⁰Japan Agency for Marine-Earth Science and Technology, Yokohama, Japan

19 **Key Points:**

- 20 • Ocean volume is a dominant control on LGM carbon sequestration and must be
21 accurately represented in models.
- 22 • Adjusting the alkalinity to account for the relative change of volume at the LGM
23 induces a large increase of oceanic carbon (of ~ 250 GtC).
- 24 • PMIP-carbon models standardly simulate high CO₂ levels (over 300 ppm) despite
25 a larger proportion of carbon in the ocean at LGM than PI.

Corresponding author: Fanny Lhardy, fanny.lhardy@lscce.ipsl.fr

Abstract

Model intercomparison studies of coupled carbon-climate simulations have the potential to improve our understanding of the processes explaining the pCO₂ drawdown at the Last Glacial Maximum (LGM) and to identify related model biases. Models participating in the Paleoclimate Modelling Intercomparison Project (PMIP) now frequently include the carbon cycle. The ongoing PMIP-carbon project provides the first opportunity to conduct multimodel comparisons of simulated carbon content for the LGM time window. However, such a study remains challenging due to differing implementation of ocean boundary conditions (e.g. bathymetry and coastlines reflecting the low sea level) and to various associated adjustments of biogeochemical variables (i.e. alkalinity, nutrients, dissolved inorganic carbon). After assessing the ocean volume of PMIP models at the pre-industrial and LGM, we investigate the impact of these modelling choices on the simulated carbon at the global scale, using both PMIP-carbon model outputs and sensitivity tests with the iLOVECLIM model. We show that the carbon distribution in reservoirs is significantly affected by the choice of ocean boundary conditions in iLOVECLIM. In particular, our simulations demonstrate a ~ 250 GtC effect of an alkalinity adjustment on carbon sequestration in the ocean. Finally, we observe that PMIP-carbon models with a freely evolving CO₂ and no additional glacial mechanisms do not simulate the pCO₂ drawdown at the LGM (with concentrations as high as 313, 331 and 315 ppm), especially if they use a low ocean volume. Our findings suggest that great care should be taken on accounting for large bathymetry changes in models including the carbon cycle.

1 Introduction

Mechanisms explaining the atmospheric CO₂ variations at the scale of glacial-interglacial cycles are not fully understood. Ice core records have shown CO₂ variations with an amplitude of about 100 ppm for the last four or five cycles (Lüthi et al., 2008). In particular, the atmospheric CO₂ is known to have reached concentrations as low as 190 ppm (Bereiter et al., 2015) at 23–19 kaBP, during the Last Glacial Maximum (LGM). Compared to pre-industrial (PI) levels of around 280 ppm, this LGM pCO₂ drawdown is commonly thought to be mainly linked to an increase in carbon sequestration in the ocean (Anderson et al., 2019).

The total carbon content of this large reservoir currently holding $\sim 38,000$ GtC (Sigman & Boyle, 2000) is influenced by both physical and biogeochemical processes (Bopp et al., 2003; Kohfeld & Ridgwell, 2009; Sigman et al., 2010; Ödalen et al., 2018). Physical processes include changes in the solubility pump: a glacial cooling is associated with higher CO₂ solubility, though counteracted by the effect of an increased salinity. They also encompass changes of Southern Ocean sea ice (Stephens & Keeling, 2000; Marzocchi & Jansen, 2019), ocean stratification (Francois et al., 1997) and circulation (Aldama-Campino et al., 2020; Ödalen et al., 2018; Watson et al., 2015; Skinner, 2009; Menviel et al., 2017; Schmittner & Galbraith, 2008). Biogeochemical processes rely on changes of the CaCO₃ cycle (Kobayashi & Oka, 2018; Matsumoto & Sarmiento, 2002; Brovkin et al., 2007, 2012) or an increased efficiency of the biological pump (Morée et al., 2021), through increased iron inputs from aeolian dust for example (Bopp et al., 2003; Tagliabue et al., 2009, 2014; Oka et al., 2011; Yamamoto et al., 2019).

Despite the identification of these processes, their contribution to the pCO₂ drawdown is still much debated. Modelling studies tend to show a large effect of the biological pump and a moderate effect of circulation changes (Khatriwala et al., 2019; Buchanan et al., 2016; Yamamoto et al., 2019; Tagliabue et al., 2009; Hain et al., 2010; Menviel et al., 2012), but model disagreements remain. Iron fertilization seems to explain a relatively small part (~ 15 ppm) of the LGM pCO₂ drawdown (Bopp et al., 2003; Tagliabue et al., 2014; Kohfeld & Ridgwell, 2009; Muglia et al., 2017). Accounting for carbonate compensation in models also seems to significantly reduce the simulated atmospheric CO₂ concentrations (Kobayashi & Oka, 2018; Brovkin et al., 2007). However,

79 review studies show that the amplitude of the CO₂ variation caused by each process is
 80 not well constrained (Kohfeld & Ridgwell, 2009; Gottschalk et al., 2020). Moreover, sen-
 81 sitivity tests underline that, due to the interactions of both these physical and biogeo-
 82 chemical processes, isolating their effect remains challenging (Hain et al., 2010; Kobayashi
 83 & Oka, 2018; Ödalen et al., 2018). The emerging common view is that the LGM pCO₂
 84 drawdown cannot be explained by a single mechanism, but by a combination of differ-
 85 ent intrinsic processes (Kohfeld & Ridgwell, 2009; Hain et al., 2010). Gaining a better
 86 understanding of these mechanisms, which depend on the background climate, is crit-
 87 ical to accurately project future climate (Yamamoto et al., 2018).

88 As a result, it is hardly surprising that models struggle to simulate the LGM pCO₂
 89 drawdown, especially in their standard version. Previous studies show that models sim-
 90 ulate a large range of pCO₂ drawdown, with most modelling studies accounting for one
 91 third to two thirds of the 90–100 ppm change inferred from ice core data (Brovkin et
 92 al., 2007, 2012; Buchanan et al., 2016; Matsumoto & Sarmiento, 2002; Hain et al., 2010;
 93 Khatiwala et al., 2019; Marzocchi & Jansen, 2019; Stephens & Keeling, 2000; Oka et al.,
 94 2011; Kobayashi & Oka, 2018; Tagliabue et al., 2009; Morée et al., 2021). The discrep-
 95 ancies between models can be partly linked to resolution (Gottschalk et al., 2020) and
 96 representation of ocean and atmosphere physics, completeness of the carbon cycle model
 97 (including sediments, permafrost...) (Kohfeld & Ridgwell, 2009), and simulated climate
 98 and ocean circulation (Menviel et al., 2017; Ödalen et al., 2018). In this context, we could
 99 learn a lot from a multimodel comparison study of standardized LGM experiments. Such
 100 studies are now common for modern and future climates: the Coupled Climate Carbon
 101 Cycle Model Intercomparison Project (C4MIP, Jones et al. (2016)) aims to quantify climate-
 102 carbon interactions in General Circulation Models (GCMs). Since the LGM is a bench-
 103 mark period of the Paleoclimate Modelling Intercomparison Project (PMIP, Kageyama
 104 et al. (2018)), the stage is set for a similar study focussed on the LGM. Indeed, the PMIP
 105 project is now in its phase 4 and a standardized experimental protocol has been designed
 106 for the LGM (Kageyama et al., 2017). Although more and more PMIP models now also
 107 simulate the carbon cycle, outputs describing the carbon cycle have not been shared through
 108 ESGF systematically and no systematic multimodel analysis of coupled climate-carbon
 109 LGM experiments has been done so far.

110 In this study, the preliminary results of the PMIP-carbon project gives us the op-
 111 portunity to examine LGM carbon outputs of a roughly consistent model ensemble for
 112 the first time. We evaluate the impact of modelling choices related to the ocean bound-
 113 ary conditions change on the simulated carbon. We assess specifically the impacts of the
 114 total ocean volume change and associated adjustments, two elements which are not the
 115 focus of the PMIP protocol. Since the PMIP-carbon project is ongoing, this first look
 116 is especially useful to draw a few conclusions which will help refine the PMIP-carbon pro-
 117 tocol.

118 **2 Modelling choices in PMIP-carbon models and resulting ocean vol-** 119 **umes**

120 **2.1 The PMIP-carbon protocol**

121 The PMIP-carbon project, which falls under the auspices of the ‘Deglaciations’ work-
 122 ing group in the PMIP structure, aims at the first multimodel comparison of coupled climate-
 123 carbon experiments at the LGM. Participating modelling groups ran both a PI and a
 124 LGM simulation with the same code, following the PMIP4 experimental design as far
 125 as possible, but model outputs obtained using the PMIP2 or PMIP3 protocol were also
 126 accepted. These standardized protocols specify modified forcing parameters (greenhouse
 127 gas concentrations and orbital parameters) and different boundary conditions (e.g. el-
 128 evation, land ice extent, coastlines, and bathymetry). Indeed, the LGM was a cold pe-
 129 riod with extensive ice sheets over the Northern Hemisphere. Due to the quantity of ice
 130 trapped on land, the eustatic sea level was around -134 m below its present value (Lambeck

131 et al., 2014). To account for the related changes of topography (which encompasses changes
 132 of elevation, albedo, coastlines and bathymetry) in models, Kageyama et al. (2017) de-
 133 fine the PMIP4 protocol and provide guidelines on how to implement the LGM bound-
 134 ary conditions on the atmosphere and ocean grids. Given the uncertainty of ice sheet
 135 reconstructions, the PMIP4 protocol lets modelling groups choose from three different
 136 topographies: GLAC-1D (Ivanovic et al., 2016), ICE-6G-C (Peltier et al., 2015; Argus
 137 et al., 2014), or PMIP3 (Abe-Ouchi et al., 2015), whereas the PMIP3 protocol relied on
 138 the PMIP3 ice sheet reconstructions ([https://wiki.lsce.ipsl.fr/pmip3/doku.php/
 139 pmip3:design:21k:final](https://wiki.lsce.ipsl.fr/pmip3/doku.php/pmip3:design:21k:final)) and the PMIP2 protocol relied on the ICE-5G one (Peltier,
 140 2004). To account for the sea level difference between the LGM and PI, the protocol un-
 141 derlines that a higher salinity of 1 psu should be ensured during the initialization of the
 142 ocean. We expect that this would partly compensate for the temperature effect by re-
 143 ducing the CO₂ solubility.

144 For ocean biogeochemistry models specifically, Kageyama et al. (2017) also recom-
 145 mend that “the global amount of dissolved inorganic carbon (DIC), alkalinity, and nu-
 146 trients should be initially adjusted to account for the change in ocean volume. This can
 147 be done by multiplying their initial value by the relative change in global ocean volume.”
 148 The implicit modelling choice here is to ensure the mass conservation of these tracers,
 149 inducing an increase of their concentration when running a LGM experiment from a PI
 150 restart. While increased nutrient concentrations can boost marine productivity and con-
 151 sequently affect the biological pump, an increase of alkalinity lowers atmospheric CO₂
 152 concentrations by displacing the acid-base equilibriums of inorganic carbon in favour of
 153 CO₃²⁻ (Sigman et al., 2010). These adjustments are typically done by assuming a 3%
 154 decrease in total ocean volume (Brovkin et al., 2007), or a decrease close to this value
 155 (Morée et al., 2021; Bouttes et al., 2010). However, it should be noted that these adjust-
 156 ments are meant to account for the sea level change at a global scale, and do not reflect
 157 local processes such as corals or shelf erosion (Broecker, 1982).

158 2.2 The PMIP-carbon model outputs

159 Four General Circulation Models (GCMs: MIROC4m-COCO, CESM, IPSL-CM5A2,
 160 MIROC-ES2L) and four Earth System Models of intermediate complexity (EMICs: CLIMBER-
 161 2, iLOVECLIM, LOVECLIM, UVic) have performed carbon-cycled enabled LGM sim-
 162 ulations submitted to the PMIP-carbon project. Most of them did not include additional
 163 glacial mechanisms (e.g. sediments, permafrost, brines, iron fertilization...) when run-
 164 ning their LGM simulation, with the exception of MIROC4m-COCO, MIROC-ES2L and
 165 IPSL-CM5A2 in which dust-induced iron fluxes were changed at the LGM. These mod-
 166 els and the characteristics of their LGM simulations are summed up in Table 1.

Table 1. Characteristics of the LGM simulations of PMIP-carbon models. * indicates that the CO₂ concentration in both the radiative and the carbon cycle code is prescribed to 190 ppm, following the PMIP4 protocol which recommended a slight change of atmospheric CO₂ (compared to 185 ppm in PMIP3) to ensure consistency with the deglaciation protocol (Ivanovic et al., 2016).

Model name	Ocean resolution lat × lon (levels)	Atmospheric CO ₂	Ice sheet reconstruction	Ocean boundary conditions	Adjustment of DIC, alkalinity, nutrients
MIROC4m	~ 1° × 1° × (43)	freely evolving	ICE-5G	unchanged	no
CLIMBER-2	2.5° × 3 basins (21)	freely evolving	ICE-5G	unchanged	yes (3.3%)
CESM	~ 400 – 40 km (60)	freely evolving	ICE-6G-C	changed	yes (5.7%)
iLOVECLIM	3° × 3° (20)	freely evolving	GLAC-1D, ICE-6G-C	changed	yes (see Sect. 3.2)
IPSL-CM5A2	2° – 0.5° (31)	prescribed*	PMIP3	changed	yes (3%)
MIROC-ES2L	1° × 1° (63)	prescribed*	ICE-6G-C	changed	yes (3%)
LOVECLIM	3° × 3° (20)	prescribed*	ICE-6G-C	unchanged	yes (3.3%)
UVic	3.6° × 1.8° (19)	prescribed*	GLAC-1D, ICE-6G-C, PMIP3	changed	no

167 This table shows that PMIP-carbon model outputs result from differing modelling
 168 choices in terms of model resolution, boundary conditions, and CO₂ forcing (either pre-
 169 scribed at 190 ppm in both the radiative code and carbon cycle model, or prescribed in
 170 the radiative code but freely evolving in the carbon cycle part). In particular, the effects
 171 of a lower sea level are accounted differently by the models. Ocean boundary conditions
 172 (i.e. bathymetry and coastlines) are not updated in three of the LGM experiments. Fur-
 173 thermore, the recommended initial adjustment of ocean biogeochemistry variables (Kageyama
 174 et al., 2017) to account for the change in ocean volume is not consistently applied. In-
 175 deed, when these three variables are adjusted, it is often according to a theoretical value
 176 of around 3%, rather than according to the relative volume change imposed in models.
 177 However, considering that the ocean boundary conditions stem from different ice sheet
 178 reconstructions and are interpolated on ocean grids of various resolution, the resulting
 179 ocean volumes and relative volume change may not always be equal to this theoretical
 180 value. These differing modelling choices give us the opportunity to evaluate their impact
 181 on the simulated carbon at the LGM.

182 2.3 The ocean volume in PMIP models

183 The total ocean volume is a variable of interest in our study: it amounts to the size
 184 of this carbon reservoir, but also conditions the adjustment of biogeochemical variables.
 185 To quantify the impact of modelling choices related to the implementation of ocean bound-
 186 ary condition on the ocean volume, we computed the ocean volumes of PMIP-carbon mod-
 187 els for both the LGM and PI period. We used the fixed fields for each model to compute
 188 the total integrated ocean volume. To provide more elements of comparison, we also com-
 189 puted the ocean volumes of additional PMIP3 models. We chose the GISS-E2-R, MRI-
 190 CGCM3, MPI-ESM-P, CNRM-CM5 and MIROC-ESM models since both their LGM and
 191 PI fixed fields were available for download.

192 The resulting values are showed in Fig. 1. They can be compared to the ocean vol-
 193 umes computed using topographic data. Indeed, topographic data are typically used to
 194 implement LGM boundary conditions (e.g. GLAC-1D, ICE-6G-C reconstructions) or PI
 195 ones (e.g. etopo1, Amante and Eakins (2009)) in models. We computed the ocean vol-
 196 ume from the ICE-6G-C and GLAC-1D topographies, both at 21 kyr and at 0 kyr (see
 197 dotted and dashed lines in Fig. 1). The ocean volume from the etopo1 topography was
 198 computed by Eakins and Sharman (2010): 1.335×10^{18} m³. These topographic data
 199 are of medium to high resolution: the ICE-6G-C topography is provided on a (1080, 2160)
 200 points grid and the GLAC-1D topography on a (360, 360) one. The etopo1 relief data
 201 have a 1 arc-minute resolution. Considering the high resolution of these data, we assume
 202 a relatively negligible error in the computed ocean volumes (with respect to reality). We
 203 use these reference values to quantify the differences linked with the interpolation on a
 204 coarser grid and/or with modelling choices made during the implementation of bound-
 205 ary conditions (Table 2).

206 We observe that the ocean volumes associated with the ICE-6G-C and GLAC-1D
 207 topographies at 0 kyr are similar to the etopo1 ocean volume (see dotted lines on Fig.
 208 1b). However, there is a difference of around 1×10^{16} m³ between the volumes com-
 209 puted at the LGM (see dashed lines on Fig. 1a and 1b): we found 1.299×10^{18} m³ (GLAC-
 210 1D), 1.292×10^{18} m³ (ICE-6G-C) and 1.288×10^{18} m³ (ICE-5G). This difference
 211 stems from the uncertainties in ice sheet reconstructions. As the Laurentide ice sheet
 212 is higher in the ICE-6G-C reconstruction than in the GLAC-1D one (Kageyama et al.,
 213 2017), the ocean volume calculated from ICE-6G-C is consistent with a lower sea level.
 214 From these reconstructions, we computed a deglacial volume gain of around 4.30×10^{16} m³
 215 (etopo1 – ICE-6G-C). We note that running LGM simulations from a PI restart (based
 216 on etopo1) entails in theory a relative volume change of -2.72% (GLAC-1D), -3.22% (ICE-
 217 6G-C), or -3.48% (ICE-5G) ; or -2.88% (GLAC-1D) and -3.19% (ICE-6G-C) when con-
 218 sidering the ICE-6G-C and GLAC-1D topographies at 0 kyr. These values are close to

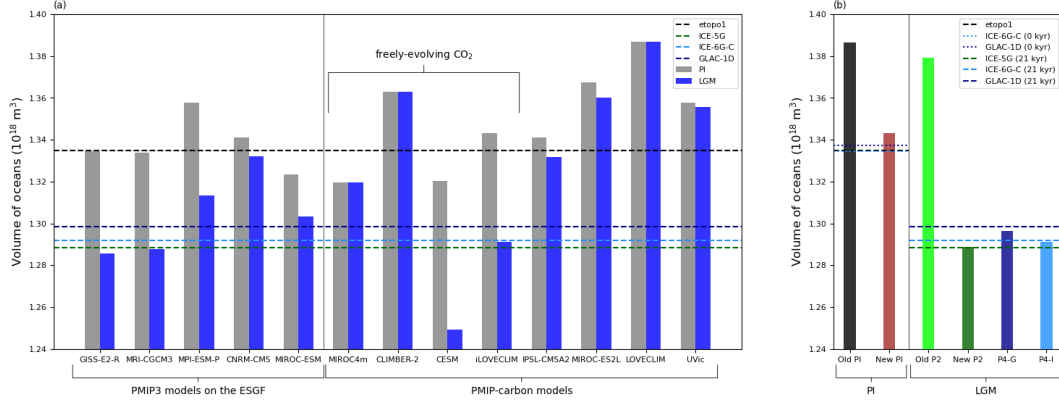


Figure 1. Ocean volume in (a) PMIP models and (b) iLOVECLIM simulations. The iLOVECLIM reference simulations in (a) are ‘New PI’ and ‘P4-I’. The dashed and dotted lines represent the ocean volume computed from high resolution topographic files (etopo1, ICE-5G, GLAC-1D, and ICE-6G-C).

Table 2. Quantification in PMIP models of ocean volumes and differences (Δ) with respect to the ocean volume computed from PI (etopo1) or from LGM topographic data (ICE-6G-C, 21 kyr). The volume changes between LGM and PI fixed fields are indicated, as well as the corresponding Δ (PI–LGM in models, compared to the etopo1–ICE-6G-C volume difference). Finally, the associated relative volume changes can be compared to the ones computed from the topographic data: -2.88% (GLAC-1D) and -3.19% (ICE-6G-C).

Model name	GISS-E2-R	MRI-CGCM3	MPI-ESM-P	CNRM-CM5	MIROC-ESM
PI (10^{18} m^3)	1.335	1.334	1.358	1.341	1.323
LGM (10^{18} m^3)	1.286	1.288	1.313	1.332	1.303
Δ PI (%)	-0.02	-0.09	+1.70	+0.47	-0.86
Δ LGM (%)	-0.48	-0.33	+1.66	+3.11	+0.88
PI–LGM (10^{16} m^3)	4.89	4.59	4.42	0.91	2.01
Δ PI–LGM (%)	+13.73	+6.92	+2.93	-78.91	-53.32
Relative change (%)	-3.66	-3.44	-3.26	-0.68	-1.52

Model name	MIROC4m	CLIMBER-2	CESM	iLOVECLIM	IPSL-CM5A2	MIROC-ES2L	LOVECLIM	UVic
PI (10^{18} m^3)	1.320	1.363	1.320	1.343	1.341	1.367	1.387	1.358
LGM (10^{18} m^3)	1.320	1.363	1.249	1.291	1.332	1.360	1.387	1.356
Δ PI (%)	-1.16	+2.10	-1.12	+0.62	+0.46	2.42	+3.90	+1.70
Δ LGM (%)	+2.13	+5.49	-3.25	-0.05	+3.08	5.26	+7.35	+4.93
PI–LGM (10^{16} m^3)	0	0	7.10	5.19	0.92	0.73	0	0.20
Δ PI–LGM (%)	-100	-100	+65.34	+20.85	-78.54	-83.09	-100	-95.33
Relative change (%)	0	0	-5.38	-3.87	-0.69	-0.53	0	-0.15

219 the 3% change enforced in the initial adjustment of biogeochemical variables in some PMIP-
 220 carbon models (Table 1).

221 We also find that PMIP models show a variety of ocean volumes (Fig. 1a and Ta-
 222 ble 2), even in their PI version. The difference with the computed volume based on high
 223 resolution topographic data (etopo1, ICE-6G-C) is significant for the majority of mod-
 224 els: this difference amounts to less than 1% for only 6 models (out of 13) at the PI and
 225 for only 4 models at the LGM. The PMIP models with an ocean volume close to the high
 226 resolution topographic data at both the PI and the LGM are MRI-CGCM3, GISS-E2-
 227 R and iLOVECLIM. MPI-ESM-P shows a slight overestimation (+1.7%) for both its PI
 228 and LGM volume but its relative volume change remains realistic (-3.26%). However,
 229 the PI–LGM difference is often largely underestimated (CNRM-CM5, MIROC-ESM,
 230 IPSL-CM5A2, MIROC-ES2L, UVic) or not implemented at all (MIROC4m-COCO, CLIMBER-

231 2, LOVECLIM). As a result, these 8 models significantly underestimate the relative vol-
 232 ume change (-0% to -1.52%). Finally, CESM underestimates both the PI and the LGM
 233 volumes while being the only model overestimating the relative volume change (-5.38%).
 234 We underline with Fig. S1 that a significantly smaller number of models also underes-
 235 timate the PI–LGM difference in ocean surface area, illustrating that the coastlines as-
 236 sociated with the low sea level of the LGM may have been set more carefully than the
 237 bathymetry.

238 We note that EMICs (CLIMBER-2, LOVECLIM, UVic) tend to significantly over-
 239 estimate the PI ocean volume with respect to etopo1 data and to show little to no change
 240 of ocean boundary conditions at the LGM. This is not the case of the iLOVECLIM model,
 241 which will be further detailed in Sect. 3.1 and in Fig. 1b. Conversely, most GCMs also
 242 show discrepancies with the ocean volumes of topographic data at both the PI and LGM
 243 (MPI-ESM-P, CESM, MIROC models) or mainly at the LGM (CNRM-CM5, IPSL-CM5A2).
 244 There is no obvious correlation between between model spatial resolution and ocean vol-
 245 ume accuracy.

246 Since PMIP-carbon models simulate various change of ocean volume, we expect dif-
 247 ferent responses of the carbon cycle to these differing ocean boundary conditions. Indeed,
 248 the carbon concentrations simulated in the ocean, which depend both on mass and vol-
 249 ume, may be merely affected by a reservoir size effect. In particular, models with a large
 250 ocean volume at the LGM may overestimate carbon storage in the ocean. Moreover, the
 251 adjustment of biogeochemical variables done in some LGM simulations (e.g. according
 252 to a theoretical -3% change) is not necessarily consistent with the ocean volume change
 253 enforced in the models. It is difficult to assess the consequences of these bathymetry re-
 254 lated modelling choices on the simulated carbon at the LGM by relying only on PMIP-
 255 carbon model outputs: these models also have differing carbon cycle modules, simulate
 256 different climate backgrounds, and do not all simulate a freely evolving CO_2 in the car-
 257 bon cycle (Table 1). Therefore, we sought to evaluate the impact of these choices using
 258 additional sensitivity tests run with the iLOVECLIM model.

259 **3 Evaluating the impact of bathymetry related modelling choices on** 260 **the simulated carbon at the LGM**

261 **3.1 Ocean boundary conditions in the iLOVECLIM model and result-** 262 **ing ocean volumes**

263 As shown in Table 1, the iLOVECLIM model ran at the LGM with a freely evolv-
 264 ing CO_2 in the carbon cycle and following the PMIP4 experimental design (Kageyama
 265 et al., 2017). We used both the GLAC-1D and the ICE-6G-C ice sheet reconstructions
 266 to implement the boundary conditions (including the bathymetry and coastlines), thanks
 267 to the new semi-automated bathymetry generation method described in Lhardy et al.
 268 (accepted, 2021). We also implemented new ocean boundary conditions for the PI, us-
 269 ing a modern high resolution topography file (etopo1) to replace the old bathymetry (adapted
 270 from etopo5, 1986). As this change of ocean boundary conditions has an impact on the
 271 ocean volume and therefore on the size of this carbon reservoir (Fig. 1b), we retuned the
 272 total carbon content at the PI in order to get an equilibrated atmospheric CO_2 concen-
 273 tration of around 280 ppm. This content is now 632 GtC lower (41,016 GtC against 41,647 GtC
 274 previously). To ensure equilibrium, we then ran 5000 years of LGM carbon simulation
 275 using this PI restart called ‘New PI’. The two standard LGM simulations (run follow-
 276 ing the PMIP4 protocol, using either the GLAC-1D or ICE-6G-C topography) are called
 277 ‘P4-G’ and ‘P4-I’ respectively. To observe the effect of the semi-automated bathymetry
 278 generation method on the ocean volume, in our study we use the fixed fields of simula-
 279 tions run with the former PI and LGM bathymetries (respectively ‘Old PI’ and ‘Old P2’).
 280 As the latter was manually generated in the framework of the PMIP2 exercise, we also
 281 regenerated with this method the bathymetry and coastlines associated with the ICE-

5G topography recommended in the PMIP2 protocol. The resulting ‘New P2’ simulation is therefore more comparable to ‘Old P2’ than the ‘P4-G’ and ‘P4-I’ simulations.

Figure 1b shows that with the implementation of manually tuned bathymetries, the former version of iLOVECLIM was run with overestimated ocean volumes at the PI (+3.86% for ‘Old PI’) and especially at the LGM (+7.06% for ‘Old P2’). Most of the overestimation of the ‘Old P2’ ocean volume is caused by differences in the deepest (deeper than 4 km) grid cells (Fig. S2), rather than the slight overestimation of the ocean surface area (Fig. S1b). As a result, iLOVECLIM used to simulate only 15% of the relative volume change (Table S1). However, we now have much more realistic ocean volume values in the current version of iLOVECLIM, both at the PI (‘New PI’) and at the two standard LGM simulations (‘P4-G’ and ‘P4-I’). Indeed, these values are all fairly close to their references (etopo1, GLAC-1D and ICE-6G-C respectively), though there is still a small overestimation of the PI ocean volume. Since we are also able to regenerate an ocean volume close to the ICE-5G one in simulation ‘New P2’, this improvement is clearly due to our new method to implement the ocean boundary conditions. Despite the interpolation of the bathymetry on a relatively coarse ocean grid, it is interesting to note that the differences (Δ) are now of the same order of magnitude than other GCMs of higher resolution (Table 1), and smaller than most models.

3.2 Modelling choices related to the boundary conditions change and set of LGM simulations with iLOVECLIM

We made several modifications to the code of iLOVECLIM to allow for a change of ocean boundary conditions in an automated way. These developments allow us to run carbon simulations with the iLOVECLIM model under any given change of ocean boundary conditions (PI, GLAC-1D, ICE-6G-C or otherwise). First, we ensured a systematic conservation of salt. Indeed, the boundary conditions changes associated with a lower glacial sea level cause a loss of the salt contained in some grid cells such as the ones corresponding to the continental shelves. In LGM runs, 1 psu is usually added to the pre-industrial salinity to compensate for this loss (Kageyama et al., 2017). We computed the total salt content before and after initialisation and the lost salt was put in the whole deep ocean (> 1 km) homogeneously. In iLOVECLIM, this automated modification is equivalent to an addition of 0.96 psu (GLAC-1D boundary conditions) or 1.11 psu (ICE-6G-C) to the pre-industrial salinity. Secondly, we coded an automated adjustment of ocean biogeochemistry variables. We chose to conserve the total alkalinity, nitrate and phosphate concentrations, and DIC, instead of multiplying their initial values by a relative volume change. This choice allows us to take into account not only the global sea level change, but also the distribution patterns of the lost tracers when the change of boundary conditions occurs. Finally, the change of bathymetry and coastlines can also cause a loss in the terrestrial biosphere carbon content or in the ocean organic carbon pools (i.e. phytoplankton, zooplankton, dissolved organic carbon, slow dissolved organic carbon, particulate organic carbon and calcium carbonate). To account for it, we ensured an automated conservation of the total carbon content. The difference between the global carbon amount before and after initialisation was put into the atmosphere, which re-equilibrates with the ocean during the run.

We aim at quantifying the impact of modelling choices which relate to the change of ocean boundary conditions on the simulated carbon, that is:

- adjustments of alkalinity, nutrients, DIC
- automated conservation of the total salt content
- automated conservation of the total carbon content, as described above

To do this, we ran sensitivity tests using the ICE-6G-C boundary conditions (like ‘P4-I’) but without one or two of these choices: these simulations are called ‘alk-’, ‘nut-’, ‘DIC-/C-’, ‘C-’ and ‘salt-’. To be clear, ‘alk’, ‘nut’ and ‘DIC’ refer to the adjustments of al-

Table 3. Bathymetry related modelling choices of the LGM simulations with iLOVECLIM. Ocean boundary conditions (BCs, i.e. coastlines, bathymetry, and the resulting ocean volume) are specified by the letters G (GLAC-1D), I (ICE-6G-C) or PI (etopo1). Crosses indicate that the automated conservation of salt and carbon and adjustment of biogeochemical variables are done according to the relative change of volume. Hyphens indicate that these adjustments are inactive due to the absence of ocean boundary conditions change. ‘no’ indicates in which simulation these adjustments are deliberately switched off and ‘yes’ when they are done according to a theoretical value (-3.22%, the relative change of volume between etopo1 and ICE-6G-C).

Simulation name	P4-G	P4-I	salt-	C-	DIC-/C-	nut-	alk-	PIbathy	PIbathy,alk+
Ocean BCs	G	I	I	I	I	I	I	PI	PI
Salt conservation	x	x	no	x	x	x	x	-	-
Carbon conservation	x	x	x	no	no	x	x	-	-
DIC adjustment	x	x	x	x	no	x	x	-	-
Nutrients adjustment	x	x	x	x	x	no	x	-	-
Alkalinity adjustment	x	x	x	x	x	x	no	-	yes

333 kalinity, nutrients and DIC, while ‘C’ refers to the total carbon content conservation and
 334 ‘salt’ to the total salt content conservation. It should be noted that we ran ‘DIC-/C-’
 335 both without the DIC adjustment and without the total carbon content conservation to
 336 be able to see the impact of the DIC adjustment, as a ‘DIC-’ simulation results in the
 337 same equilibrium state of the carbon cycle as the reference ‘P4-I’, albeit after a longer
 338 equilibration time. Indeed, the total carbon content conservation – ensured by trans-
 339 ferring the lost carbon to the atmosphere – makes up for the missing DIC adjustment,
 340 though the ocean and atmosphere need more time to re-equilibrate.

341 As the ocean boundary conditions are not always implemented in LGM simulations
 342 of PMIP-carbon models, we also ran a LGM simulation with the PI coastlines and bathymetry
 343 (called ‘PIbathy’). As a consequence, there was no change of ocean volume nor any ad-
 344 justment of biogeochemical variables during the initialization of this simulation. Finally,
 345 this ensemble of simulations is completed by ‘PIbathy, alk+’. In this LGM simulation
 346 with the PI ocean boundary conditions, we increased the initial alkalinity according to
 347 a theoretical relative change of volume, since this is a modelling choice of some PMIP-
 348 carbon models. All simulations and the modelling choices related to the change of bound-
 349 ary conditions are summed up in Table 3.

350 3.3 Simulated carbon at the LGM

351 To assess the impact on the simulated carbon of these modelling choices which relates
 352 to the change of ocean boundary conditions, we computed the carbon content of
 353 each carbon reservoir (atmosphere, ocean, terrestrial biosphere) in PMIP-carbon mod-
 354 els and iLOVECLIM sensitivity tests. Typically for the ocean, the concentration in each
 355 carbon pool (e.g. DIC, dissolved organic carbon, particulate carbon, phytoplankton...) was
 356 summed, integrated on the ocean grid (weighted by the grid cell volume), and con-
 357 verted into GtC. The equilibrated atmospheric CO₂ concentrations of PMIP-carbon mod-
 358 els with freely evolving CO₂ in the carbon cycle are presented in Fig. 2a. The interested
 359 reader will find the carbon content of all reservoirs and models in Fig. S3.

360 Among the PMIP-carbon models, only half have thus far run with a freely evol-
 361 ving CO₂ for the carbon cycle (MIROC4m-COCO, CLIMBER-2, CESM and iLOVECLIM).
 362 Furthermore, among this subset, only CESM and iLOVECLIM are fully comparable in
 363 terms of carbon outputs, as they both have run with LGM ocean boundary conditions
 364 and include a vegetation model. We observe that these two models both typically sim-
 365 ulate high CO₂ concentrations at the LGM (331 ppm and 315 ppm respectively, see Fig. 2a).
 366 These values do not compare well with the CO₂ levels inferred from data (~190 ppm,
 367 Bereiter et al. (2015)) as they are even higher than the PI levels (280 ppm).

3.3.1 In iLOVECLIM

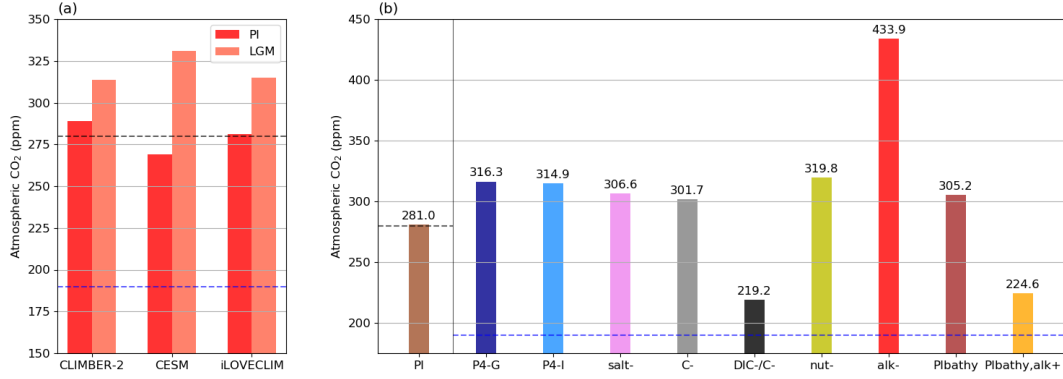


Figure 2. Atmospheric CO₂ (ppm) in (a) PMIP-carbon models with a freely evolving CO₂ in the carbon cycle (excluding the ocean-only MIROC4m-COCO) and (b) iLOVECLIM simulations. The iLOVECLIM reference simulations in (a) are ‘New PI’ and ‘P4-I’. The grey and blue dashed lines represents the atmospheric CO₂ concentrations at the PI (280 ppm) and LGM (190 ppm, Bereiter et al. (2015)).

Table 4. Quantification in iLOVECLIM simulations of the carbon content in reservoirs (GtC) and differences (GtC) with respect to ‘P4-I’

Simulation name	New PI	P4-G	P4-I	salt-	C-	DIC-/C-	nut-	alk-	PIbathy	PIbathy,alk+
Atmosphere (GtC)	599	674	671	653	643	467	681	924	650	478
Ocean (GtC)	38,480	38,768	38,753	38,767	38,627	37,599	38,742	38,499	39,020	39,191
Vegetation (GtC)	1,937	1,615	1,593	1,596	1,593	1,593	1,593	1,593	1,347	1,347
Atmosphere difference	-72	+3	0	-18	-28	-204	+10	+254	-21	-192
Ocean difference	-272	-25	0	+14	-126	-1153	-10	-253	+267	+439
Vegetation difference	+344	+22	0	+3	0	0	0	0	-246	-246

369 Looking at the carbon distribution simulated in the different reservoirs by the iLOVE-
 370 CLIM model (Table 4), we observe that although the ocean volume is smaller, the ocean
 371 is effectively trapping more carbon at the LGM (+272 GtC for ‘P4-I’ compared to ‘New PI’).
 372 However, the terrestrial biosphere sink is also less efficient due to lower temperatures and
 373 the presence of large ice sheets (-344 GtC). Overall, it results in higher atmospheric con-
 374 centrations as the ocean sink is not enhanced enough to compensate the lower terres-
 375 trial biosphere sink. The carbon outputs from the two standard LGM simulations (‘P4-
 376 G’ and ‘P4-I’) suggest that the ice sheet reconstruction (GLAC-1D or ICE-6G-C) chosen
 377 to implement the boundary conditions has a small impact on the simulated carbon
 378 (as well as the ocean volume, see Fig. 1b and Table S1).

379 Using the iLOVECLIM sensitivity tests, we quantify the carbon content variations
 380 associated with the modelling choices made to accommodate the change of ocean bound-
 381 ary conditions. If the total salt content conservation is not ensured (‘salt-’), we get slightly
 382 lower CO₂ concentrations (8 ppm lower), as the CO₂ solubility is greater when the salin-
 383 ity is lower. The total carbon content conservation apparently has a relatively small ef-
 384 fect on the CO₂ (13 ppm lower), but is actually essential when the DIC adjustment is
 385 not done either (‘DIC-/C-’): in this case, 1,357 GtC are lost, and the CO₂ concentra-
 386 tion is much closer to the LGM data value but for the wrong reason, that is a loss of to-
 387 tal carbon from the system. Only 154 GtC are lost in the ‘C-’ simulation, which amount
 388 to the lost organic carbon. Indeed, the DIC adjustment compensates for most of the lost

389 carbon as the DIC is the largest carbon pool in the ocean. As for the other two recom-
 390 mended adjustments, the nutrient adjustment has a relatively small effect through a ma-
 391 rine productivity boost (+5 ppm without it, see ‘nut-’) whereas the alkalinity adjustment
 392 is much more critical. Indeed, the simulation without it (‘alk-’) has a CO₂ reaching as
 393 high as 434 ppm: an increased alkalinity reduces the atmospheric CO₂ concentration (by
 394 254 GtC). Given the large effect of this adjustment, the method used to implement it
 395 is crucial.

396 In addition, we quantify the carbon content simulated at the LGM with no change
 397 of ocean boundary conditions in iLOVECLIM. We see from the ‘PIbathy’ simulation that
 398 a larger ocean volume can significantly increase the ocean carbon content at the LGM
 399 (+267 GtC, close to a doubling of the PI–LGM difference), but in this instance at the
 400 expense of the terrestrial carbon (-246 GtC). This difference in terrestrial carbon con-
 401 tent can be explained by the second ocean boundary condition, as the PI coastlines yield
 402 less available land surfaces to grow vegetation. While this compensation of errors causes
 403 a relatively small change of atmospheric CO₂ concentration, we argue here that not chang-
 404 ing the bathymetry while performing LGM experiments significantly affects the carbon
 405 distribution since it can potentially trap twice as much carbon in the ocean. Further-
 406 more, if this absence of ocean boundary conditions change is combined with the adjust-
 407 ment of alkalinity (considering the theoretical relative volume change between etop1
 408 and ICE-6G-C, see ‘PIbathy,alk+’), the carbon storage of the ocean is increased even
 409 more. This time, the drop of atmospheric CO₂ concentration is much more significant
 410 as there is no additional compensating effect of the terrestrial biosphere.

411 3.3.2 In PMIP-carbon models

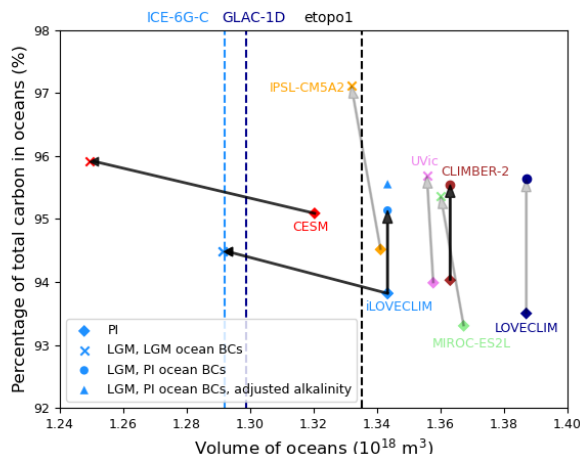


Figure 3. Ocean carbon versus ocean volume plot for a subset of PMIP-carbon models (excluding the ocean-only MIROC4m-COCO) and iLOVECLIM simulations (‘P4-I’, ‘PIbathy’ and ‘PIbathy,alk+’). The dashed lines represent the ocean volume computed from high resolution topographic files (etop1, GLAC-1D, ICE-6G-C). The PI to LGM changes are traced by the grey (prescribed CO₂) and black (freely evolving CO₂) arrows.

412 Finally, since the ocean is thought to have played a major role in explaining the
 413 pCO₂ drawdown at the LGM, we now examine the ocean carbon content simulated by
 414 PMIP-carbon models in light of our findings on ocean volume. We know that PMIP-carbon
 415 models simulate various total carbon content (Fig. S3b). To be able to compare their
 416 carbon content in the ocean, we therefore plotted in Fig. 3 the percentage of carbon in
 417 the ocean at the PI and LGM, against the ocean volume. Figure 3 clearly shows three
 418 distinct model behaviours. CLIMBER-2 and LOVECLIM, which have run with no change

419 of ocean boundary conditions, show a significantly larger proportion of carbon in the oceans
 420 under LGM conditions (+1.5% and +2.1% respectively). IPSL-CM5A2, MIROC-ES2L
 421 and UVic have run with a limited change of ocean volume, and they also simulate a large
 422 increase of carbon storage in the oceans between their PI and LGM states (+2.6%, +2.1%
 423 and 1.7% respectively). In contrast, the ocean carbon content of iLOVECLIM and CESM
 424 increases at the LGM, but this variation (+0.7% and +0.8%) is relatively smaller than
 425 in other models with no large change of ocean boundary conditions. Besides, the two iLOVE-
 426 CLIM simulations with no change of ocean volume show a larger increase of carbon stor-
 427 age in the oceans (+1.3% and +1.7% for ‘PIbathy’ and ‘PIbathy,alk+’ respectively). There-
 428 fore, it is likely that other models would also simulate lower carbon sequestration in the
 429 oceans and high atmospheric CO₂ concentration values (much larger than 190 ppm) if
 430 they had a lower ocean volume at the LGM.

431 **4 Conclusion**

432 In this study, we use preliminary results of the PMIP-carbon project and sensitiv-
 433 ity tests run with the iLOVECLIM model at the LGM to quantify the consequences of
 434 bathymetry related modelling choices on the simulated carbon at the global scale. We
 435 consider the effects of the ocean volume change and of the resulting biogeochemical vari-
 436 ables adjustments recommended in Kageyama et al. (2017).

437 We show that the implementation of ocean boundary conditions in PMIP models
 438 rarely results in accurate ocean volumes. We suggest that this may not be primarily re-
 439 lated to the model resolution, since we get a much more realistic ocean volume in iLOVE-
 440 CLIM after developing a new method to generate the bathymetry despite the relatively
 441 coarse resolution of its ocean model. In fact, the ocean boundary conditions (i.e. bathymetry,
 442 coastlines) associated with the low sea level of the LGM are not systematically gener-
 443 ated in models. When they are, modelling groups often mostly concentrate on setting
 444 the coastlines (“land-sea mask”) and the bathymetry of shallow grid cells in order to sim-
 445 ulate a reasonable ocean circulation. However, the ocean volume is mostly affected by
 446 the bathymetry of deep grid cells in models with irregular vertical levels. Setting the bathymetry
 447 of these deep grid cells to account for a sea level of -134 m (Lambeck et al., 2014) at the
 448 LGM, even if the vertical resolution exceeds such a value, will move up the ocean floor
 449 here and there depending on the outcome of vertical interpolation. As a result, the over-
 450 all volume of deep levels should be closer to reality.

451 While these modelling choices may have little consequences on the climate variables
 452 usually examined in PMIP intercomparison papers, we argue that their effects on the
 453 simulated carbon cannot be overlooked, considering the role of the deep ocean on car-
 454 bon storage (Skinner, 2009). In the iLOVECLIM model, the carbon distribution in reser-
 455 voirs is significantly affected when the low sea level is not taken into account. Indeed,
 456 in the absence of a change of ocean boundary conditions in LGM runs, the carbon se-
 457 questration in the ocean is increased twofold due to the larger size of this reservoir. In
 458 contrast, more carbon is lost in the terrestrial biosphere as the coastlines of the PI do
 459 not allow for emerged continental shelves to grow vegetation. While different model bi-
 460 ases may limit carbon sequestration in the ocean (e.g. underestimated stratification, sea
 461 ice, efficiency of the biological pump), an overestimated ocean volume at the LGM has
 462 an opposite effect. It is therefore even more challenging for models with a realistic ocean
 463 volume at the LGM to simulate the pCO₂ drawdown.

464 Kageyama et al. (2017) recommend an adjustment of DIC, nutrients and alkalini-
 465 ty to account for the change of ocean volume between the PI and the LGM. We quan-
 466 tify the effects of each on the simulated carbon at the LGM in the iLOVECLIM model.
 467 The DIC adjustment shortens the equilibration time but is not essential as long as car-
 468 bon conservation is otherwise ensured. We observe a limited effect of the nutrients ad-
 469 justment but adjusting the alkalinity yields a large increase of carbon sequestration in
 470 the ocean (~ 250 GtC). As a result, this last adjustment should be cautiously made.
 471 Multiplying the initial alkalinity by a theoretical value of around 3% which is potentially

472 far from the implemented relative change of volume can significantly decrease the atmo-
473 spheric CO₂ concentration.

474 The quantified effects of these modelling choices in iLOVECLIM depend on the car-
475 bon cycle module and on the simulated climate (e.g. surface temperatures, deep ocean
476 circulation, sea ice). In that respect, quantifications using other models would be use-
477 ful to assess the robustness of these results, which can be affected by model biases. Fur-
478 ther studies using coupled carbon-climate models including sediments may be especially
479 desirable to be able to compute the alkalinity budget from riverine inputs and CaCO₃
480 burial (Sigman et al., 2010), as accounting for this mechanism may significantly increase
481 the simulated pCO₂ drawdown (Brovkin et al., 2007, 2012; Kobayashi & Oka, 2018) .
482 Still, these results give us a sense of the magnitude of each effect. We stress here that
483 the ocean volume and the alkalinity adjustment should be both carefully considered in
484 coupled carbon-climate simulations at the LGM as there is a risk of simulating a low CO₂
485 for the wrong reasons.

486 At present, PMIP-carbon models with a freely evolving CO₂ are all simulating an
487 increased carbon sequestration into the ocean at the LGM, but also high atmospheric
488 concentrations (> 300 ppm). Overall, the enhanced carbon sink of the ocean is there-
489 fore not compensating for the loss of carbon in the terrestrial biosphere due to the lower
490 temperatures and extensive ice sheets. Causes for the glacial CO₂ drawdown can be sought
491 inside (e.g. physical and biogeochemical biases, Morée et al. (2021)) or outside (e.g. iron,
492 terrestrial vegetation, sediments, permafrost) of the modelled ocean. However, investi-
493 gating the processes behind the pCO₂ drawdown at the LGM and their limitations in
494 model representation remains a challenge insofar as model outputs are hardly compa-
495 rable. Our findings emphasize the need of documenting the ocean volume in models and
496 defining a stricter protocol for PMIP-carbon models in the view of improving coupled
497 climate-carbon simulations intercomparison potential. Explicit guidelines concerning the
498 change of ocean volume and related modelling choices (e.g. adjustment of biogeochem-
499 ical variables) may also be relevant for other target periods of paleoclimate modelling.

500 **Appendix A Description of the iLOVECLIM model under the PMIP** 501 **experimental design**

502 The iLOVECLIM model (Goosse et al., 2010) is an EMIC. Its standard version in-
503 cludes an atmospheric component (ECBilt), a simple land vegetation module (VECODE)
504 and an ocean general circulation model named CLIO, of relatively coarse resolution (3° × 3°
505 and 20 irregular vertical levels). In addition, a carbon cycle model is fully coupled to these
506 components. Originated from a NPZD ecosystem model (Six & Maier-Reimer, 1996),
507 it was further developed in the CLIMBER-2 model (Brovkin, Bendtsen, et al., 2002;
508 Brovkin, Hofmann, et al., 2002; Brovkin et al., 2007) before it was also implemented in
509 iLOVECLIM (Bouttes et al., 2015).

510 The iLOVECLIM model is typically used to simulate past climates such as the LGM,
511 and contributed to previous PMIP exercises (Roche et al., 2012; Otto-Bliesner et al., 2007)
512 under its PMIP2 version (Roche et al., 2007), as well as to the current PMIP4 exercise
513 (Kageyama et al., accepted, 2021). The LGM simulations run with iLOVECLIM follow
514 the standardized experimental design described in the PMIP4 protocol (Kageyama et
515 al., 2017). In order to assess the impact of the ice sheet reconstruction choice, we im-
516 plemented the boundary conditions associated with the two most recent reconstructions
517 (GLAC-1D and ICE-6G-C, both recommended in Ivanovic et al. (2016)) in the iLOVE-
518 CLIM model, using a new semi-automated bathymetry generation method described in
519 Lhardy et al. (accepted, 2021). The change of bathymetry and coastlines was automated
520 for the most part, with a few unavoidable manual changes in straits and key passages.
521 We also implemented new ocean boundary conditions for the PI, using a modern high
522 resolution topography file (etopo1, Amante and Eakins (2009)) to replace the old bathymetry
523 (adapted from etopo5, 1986).

524 **Acknowledgments**

525 The model outputs of PMIP-carbon models and iLOVECLIM simulations are avail-
 526 able for download online (doi: 10.5281/zenodo.4742526). The fixed fields of GISS-E2-
 527 R, MRI-CGCM3, MPI-ESM-P, CNRM-CM5 and MIROC-ESM models can also be found
 528 at <https://esgf-node.llnl.gov/projects/cmip5/>. Descriptions of the PMIP-carbon
 529 models can be found in Kobayashi and Oka (2018) (MIROC4m-COCO), Petoukhov et
 530 al. (2000) and Ganopolski et al. (2001) (CLIMBER), Bouttes et al. (2015) and Lhardy
 531 et al. (accepted, 2021) (iLOVECLIM), Ohgaito et al. (2021) and Hajima et al. (2020)
 532 (MIROC-ES2L).

533 FL, NB and DMR designed the research. NB coordinated the PMIP-carbon project
 534 and obtained funding. Participating modelling groups all performed a PI and a LGM
 535 simulation, provided their model outputs and the relevant metadata and computed the
 536 equilibrated carbon content in reservoirs. These modelling groups included AA-O, HK
 537 and AO (MIROC4m-COCO) ; KC (CLIMBER-2) ; MJ, RN, GV and ZC (CESM) ; MK
 538 (IPSL-CM5A2) ; AY (MIROC-ES2L) ; LM (LOVECLIM) ; JM and AS (UVic). FL, DMR
 539 and NB generated new boundary conditions in the iLOVECLIM model. NB and DMR
 540 developed the automated adjustments to allow for a change of ocean boundary condi-
 541 tions. FL ran the iLOVECLIM simulations and analyzed both the iLOVECLIM and the
 542 PMIP-carbon outputs under supervision of NB and DMR. FL wrote the manuscript with
 543 the inputs from all co-authors.

544 This study was supported by the French National program LEFE (*Les Enveloppes*
 545 *Fluides et l'Environnement*). FL is supported by the *Université Versailles Saint-Quen-*
 546 *tin-en-Yvelines* (UVSQ). NB and DMR are supported by the *Centre national de la recherche*
 547 *scientifique* (CNRS). In addition, DMR is supported by the Vrije Universiteit Amster-
 548 dam. LM acknowledges funding from the Australian Research Council grant FT180100606.
 549 AY acknowledges funding from the Integrated Research Program for Advancing Climate
 550 Models (TOUGOU) Grant Number JPMXD0717935715 from the Ministry of Education,
 551 Culture, Sports, Science and Technology (MEXT), Japan. We acknowledge the use of
 552 the LSCE storage and computing facilities. We thank Théo Mandonnet for his prelim-
 553 inary work on the PMIP-carbon project.

554 The authors declare that they have no conflict of interest.

555 **References**

- 556 Abe-Ouchi, A., Saito, F., Kageyama, M., Braconnot, P., Harrison, S. P., Lambeck,
 557 K., ... Takahashi, K. (2015). Ice-sheet configuration in the CMIP5/PMIP3
 558 Last Glacial Maximum experiments. *Geosci. Model Dev.*, 8, 3621–3637. doi:
 559 10.5194/gmd-8-3621-2015
- 560 Aldama-Campino, A., Fransner, F., Ödalen, M., Groeskamp, S., Yool, A., Döös,
 561 K., & Nycander, J. (2020). Meridional Ocean Carbon Transport. *Global*
 562 *Biogeochem. Cy.*. doi: 10.1029/2019GB006336
- 563 Amante, C., & Eakins, B. W. (2009). ETOPO1 1 Arc-Minute Global Relief Model:
 564 Procedures, Data Sources and Analysis. NOAA Technical Memorandum
 565 NESDIS NGDC-24. National Geophysical Data Center, NOAA. [https://](https://www.ngdc.noaa.gov/mgg/global/global.html)
 566 www.ngdc.noaa.gov/mgg/global/global.html. doi: 10.7289/V5C8276M
- 567 Anderson, R. F., Sachs, J. P., Fleisher, M. Q., Allen, K. A., Yu, J., Koutavas, A., &
 568 Jaccard, S. L. (2019). Deep-Sea Oxygen Depletion and Ocean Carbon Seques-
 569 tration During the Last Ice Age. *Global Biogeochem. Cy.*, 33, 301–317. doi:
 570 10.1029/2018GB006049
- 571 Argus, D. F., Peltier, W. R., Drummond, R., & Moore, A. W. (2014). The Antarc-
 572 tica component of postglacial rebound model ICE-6G-C (VM5a) based on
 573 GPS positioning, exposure age dating of ice thicknesses, and relative sea
 574 level histories. *Geophysical Journal International*, 198, 537–563. doi:
 575 10.1093/gji/ggu140

- 576 Bereiter, B., Eggleston, S., Schmitt, J., Nehrbass-Ahles, C., Stocker, T. F., Fischer,
577 H., ... Chappellaz, J. (2015). Revision of the EPICA Dome C CO₂ record
578 from 800 to 600 kyr before present. *Geophys. Res. Lett.*, *42*, 542–549. doi:
579 10.1002/2014GL061957
- 580 Bopp, L., Kohfeld, K. E., & Le Quéré, C. (2003). Dust impact on marine biota and
581 atmospheric CO₂ during glacial periods. *Paleoceanography*, *18*(2). doi: 10
582 .1029/2002PA000810
- 583 Bouttes, N., Paillard, D., & Roche, D. M. (2010). Impact of brine-induced stratifica-
584 tion on the glacial carbon cycle. *Clim. Past*, *6*(5), 575–589. doi: 10.5194/cp-6
585 -575-2010
- 586 Bouttes, N., Roche, D. M., Mariotti, V., & Bopp, L. (2015). Including an ocean car-
587 bon cycle model into iLOVECLIM (v1.0). *Geoscientific Model Development*, *8*,
588 1563–1576. doi: 10.5194/gmd-8-1563-2015
- 589 Broecker, W. S. (1982). Ocean chemistry during glacial time. *Geochimica et Cos-
590 mochimica Acta*, *46*, 1689–1705.
- 591 Brovkin, V., Bendtsen, J., Claussen, M., Ganopolski, A., Kubatzki, C., Petoukhov,
592 V., & Andreev, A. (2002). Carbon cycle, vegetation, and climate dynamics in
593 the Holocene: Experiments with the CLIMBER-2 model. *Global Biogeochem.
594 Cy.*, *16*. doi: 10.1029/2001GB001662
- 595 Brovkin, V., Ganopolski, A., Archer, D., & Munhoven, G. (2012). Glacial CO₂ cy-
596 cle as a succession of key physical and biogeochemical processes. *Clim. Past*,
597 *8*, 251–264. doi: 10.5194/cp-8-251-2012
- 598 Brovkin, V., Ganopolski, A., Archer, D., & Rahmstorf, S. (2007). Lowering of glacial
599 atmospheric CO₂ in response to changes in oceanic circulation and marine
600 biogeochemistry. *Paleoceanography*, *22*(PA4202). doi: 10.1029/2006PA001380
- 601 Brovkin, V., Hofmann, M., Bendtsen, J., & Ganopolski, A. (2002). Ocean biol-
602 ogy could control atmospheric $\delta^{13}\text{C}$ during glacial-interglacial cycle. *Geochem.
603 Geophys. Geosyst.*, *3*(1027). doi: 10.1029/2001GC000270
- 604 Buchanan, P. J., Matear, R. J., Lenton, A., Phipps, S. J., Chase, Z., & Etheridge,
605 D. M. (2016). The simulated climate of the Last Glacial Maximum and in-
606 sights into the global marine carbon cycle. *Clim. Past*, *12*, 2271–2295. doi:
607 10.5194/cp-12-2271-2016
- 608 Eakins, B., & Sharman, G. (2010). Volumes of the World’s Oceans from ETOPO1.
609 Retrieved from [https://ngdc.noaa.gov/mgg/global/etopo1_ocean_volumes](https://ngdc.noaa.gov/mgg/global/etopo1_ocean_volumes.html)
610 [.html](https://ngdc.noaa.gov/mgg/global/etopo1_ocean_volumes.html)
- 611 Francois, R., Altabet, M. A., Yu, E.-F., Sigman, D. M., Bacon, M. P., Frankk, M.,
612 ... Labeyrie, L. D. (1997). Contribution of Southern Ocean surface-water
613 stratification to low atmospheric CO₂ concentrations during the last glacial
614 period. *Nature*, *389*, 929–935.
- 615 Ganopolski, A., Petoukhov, V., Rahmstorf, S., Brovkin, V., Claussen, M., Eliseev,
616 A., & Kubatzki, C. (2001). CLIMBER-2: a climate system model of intermedi-
617 ate complexity. Part II: model sensitivity. *Climate Dynamics*, *17*(10), 735–751.
618 doi: 10.1007/S003820000144
- 619 Goosse, H., Brovkin, V., Fichefet, T., Haarsma, R., Huybrechts, P., Jongma, J., ...
620 Weber, S. L. (2010). Description of the Earth system model of intermediate
621 complexity LOVECLIM version 1.2. *Geoscientific Model Development*, *3*(2),
622 603–633. doi: 10.5194/gmd-3-603-2010
- 623 Gottschalk, J., Battaglia, G., Fischer, H., Frölicher, T. L., Jaccard, S. L., Jeltsch-
624 Thömmes, A., ... Thomas F. Stocker, T. F. (2020). Mechanisms of millennial-
625 scale atmospheric CO₂ change in numerical model simulations. *Quaternary
626 Science Reviews*, 30–74. doi: 10.1016/j.quascirev.2019.05.013
- 627 Hain, M. P., Sigman, D. M., & Haug, G. H. (2010). Carbon dioxide effects of
628 Antarctic stratification, North Atlantic Intermediate Water formation, and
629 subantarctic nutrient drawdown during the last ice age: Diagnosis and synthe-
630 sis in a geochemical box model. *Global Biogeochem. Cy.*, *24*(GB4023). doi:

- 631 10.1029/2010GB003790
- 632 Hajima, T., Watanabe, M., Yamamoto, A., Tatebe, H., Noguchi, M. A., Abe, M., ...
633 Kawamiya, M. (2020). Development of the MIROC-ES2L Earth system model
634 and the evaluation of biogeochemical processes and feedbacks. *Geosci. Model*
635 *Dev.*, *13*, 2197–2244. doi: 10.5194/gmd-13-2197-2020
- 636 Ivanovic, R. F., Gregoire, L. J., Kageyama, M., Roche, D. M., Valdes, P. J., Burke,
637 A., ... Tarasov, L. (2016). Transient climate simulations of the deglacia-
638 tion 21–9 thousand years before present (version 1) PMIP4 Core experiment
639 design and boundary conditions. *Geosci. Model Dev.*, *9*, 2563–2587. doi:
640 10.5194/gmd-9-2563-2016
- 641 Jones, C. D., Arora, V., Friedlingstein, P., Bopp, L., Brovkin, V., Dunne, J., ...
642 Zaehle, S. (2016). C4MIP The Coupled ClimateCarbon Cycle Model Inter-
643 comparison Project: experimental protocol for CMIP6. *Geosci. Model Dev.*, *9*,
644 2853–2880. doi: 10.5194/gmd-9-2853-2016
- 645 Kageyama, M., Albani, S., Braconnot, P., Harrison, S. P., Hopcroft, P. O., Ivanovic,
646 R. F., ... Zheng, W. (2017). The PMIP4 contribution to CMIP6 Part 4: Sci-
647 entific objectives and experimental design of the PMIP4-CMIP6 Last Glacial
648 Maximum experiments and PMIP4 sensitivity experiments. *Geoscientific*
649 *Model Development*, *10*, 4035–4055. doi: 10.5194/gmd-10-4035-2017
- 650 Kageyama, M., Braconnot, P., Harrison, S. P., Haywood, A. M., Jungclauss, J. H.,
651 Otto-Bliesner, B. L., ... Zhou, T. (2018). The PMIP4 contribution to CMIP6
652 Part 1: Overview and over-arching analysis plan. *Geoscientific Model Develop-*
653 *ment*, *11*, 1033–1057. doi: 10.5194/gmd-11-1033-2018
- 654 Kageyama, M., Harrison, S. P., Kapsch, M.-L., Löfverström, M., Lora, J. M., Miko-
655 lajewicz, U., ... Volodin, E. (accepted, 2021). The PMIP4-CMIP6 Last
656 Glacial Maximum experiments: preliminary results and comparison with the
657 PMIP3-CMIP5 simulations. *Clim. Past*. doi: 10.5194/cp-2019-169
- 658 Khatiwala, S., Schmittner, A., & Muglia, J. (2019). Air-sea disequilibrium enhances
659 ocean carbon storage during glacial periods. *Sci. Adv.*, *5*(6). doi: 10.1126/
660 sciadv.aaw4981
- 661 Kobayashi, H., & Oka, A. (2018). Response of Atmospheric pCO₂ to Glacial
662 Changes in the Southern Ocean Amplified by Carbonate Compensation.
663 *Paleoceanography and Paleoclimatology*, *33*, 1206–1229. doi: 10.1029/
664 2018PA003360
- 665 Kohfeld, K. E., & Ridgwell, A. (2009).
666 In *Surface ocean-lower atmosphere processes, volume 187* (chap. Glacial-
667 interglacial variability in atmospheric CO₂). doi: 10.1029/2008GM000845
- 668 Lambeck, K., Rouby, H., Purcell, A., Sun, Y., & Sambridge, M. (2014). Sea level
669 and global ice volumes from the Last Glacial Maximum to the Holocene. *Pro-*
670 *ceedings of the National Academy of Sciences*, *111*(43), 15296–15303. doi: 10
671 .1073/pnas.1411762111
- 672 Lhardy, F., Bouttes, N., Roche, D. M., Crosta, X., Waelbroeck, C., & Paillard,
673 D. (accepted, 2021). Impact of Southern Ocean surface conditions on deep
674 ocean circulation at the LGM: a model analysis. *Climate of the Past*. doi:
675 10.5194/cp-2020-148
- 676 Lüthi, D., Le Floch, M., Bereiter, B., Blunier, T., Barnola, J.-M., Siegenthaler,
677 U., ... Stocker, T. F. (2008). High-resolution carbon dioxide concentration
678 record 650,000–800,000 years before present. *Nature*, *453*, 379–382. doi:
679 10.1038/nature06949
- 680 Marzocchi, A., & Jansen, M. F. (2019). Global cooling linked to increased glacial
681 carbon storage via changes in Antarctic sea ice. *Nature geoscience*, *12*, 1001-
682 1005. doi: 10.1038/s41561-019-0466-8
- 683 Matsumoto, K., & Sarmiento, J. L. (2002). Silicic acid leakage from the South-
684 ern Ocean: A possible explanation for glacial atmospheric pCO₂. *Global Bio-*
685 *geochem. Cy.*, *16*(3). doi: 10.1029/2001GB001442

- 686 Menviel, L., Joos, F., & Ritz, S. P. (2012). Simulating atmospheric CO₂, ¹³C and
 687 the marine carbon cycle during the Last Glacial-Interglacial cycle: possible
 688 role for a deepening of the mean remineralization depth and an increase in
 689 the oceanic nutrient inventory. *Quaternary Science Reviews*, *56*, 46–68. doi:
 690 10.1016/j.quascirev.2012.09.012
- 691 Menviel, L., Yu, J., Joos, F., Mouchet, A., Meissner, K. J., & England, M. H.
 692 (2017). Poorly ventilated deep ocean at the Last Glacial Maximum inferred
 693 from carbon isotopes: A data-model comparison study. *Paleoceanography*, *32*,
 694 2–17. doi: 10.1002/2016PA003024
- 695 Morée, A. L., Schwinger, J., Ninnemann, U. S., Jeltsch-Thömmes, A., Bethke,
 696 I., & Heinze, C. (2021). Evaluating the biological pump efficiency of the
 697 Last Glacial Maximum ocean using $\delta^{13}\text{C}$. *Clim. Past*, *17*, 753–774. doi:
 698 10.5194/cp-17-753-2021
- 699 Muglia, J., Somes, C. J., Nickelsen, L., & Schmittner, A. (2017). Combined Effects
 700 of Atmospheric and Seafloor Iron Fluxes to the Glacial Ocean. *Paleoceanogra-*
 701 *phy*, *32*. doi: 10.1002/2016PA003077
- 702 Ödalen, M., Nycander, J., Oliver, K. I. C., Brodeau, L., & Ridgwell, A. (2018).
 703 The influence of the ocean circulation state on ocean carbon storage and CO₂
 704 drawdown potential in an Earth system model. *Biogeosciences*, *15*, 1367–1393.
 705 doi: 10.5194/bg-15-1367-2018
- 706 Ohgaito, R., Yamamoto, A., Hajima, T., Oishi, R., Abe, M., Tatebe, H., ...
 707 Kawamiya, M. (2021). PMIP4 experiments using MIROC-ES2L Earth system
 708 model. *Geosci. Model Dev.*, *14*, 1195–1217. doi: 10.5194/gmd-14-1195-2021
- 709 Oka, A., Abe-Ouchi, A., Chikamoto, M. O., & Ide, T. (2011). Mechanisms con-
 710 trolling export production at the LGM: Effects of changes in oceanic physical
 711 fields and atmospheric dust deposition. *Global Biogeochem. Cy.*, *25*(GB2009).
 712 doi: 10.1029/2009GB003628
- 713 Otto-Bliesner, B. L., Hewitt, C. D., Marchitto, T. M., Brady, E., Abe-Ouchi, A.,
 714 Crucifix, M., ... Weber, S. L. (2007). Last Glacial Maximum ocean ther-
 715 mohaline circulation: PMIP2 model intercomparisons and data constraints.
 716 *Geophys. Res. Lett.*, *34*(12), 1–6. doi: 10.1029/2007GL029475
- 717 Peltier, W. R. (2004). Global glacial isostasy and the surface of the ice-age Earth:
 718 the ICE-5G (VM2) model and GRACE. *Annual Review of Earth and Plane-*
 719 *tary Sciences*, *32*, 111–149. doi: 10.1146/annurev.earth.32.082503.144359
- 720 Peltier, W. R., Argus, D. F., & Drummond, R. (2015). Space geodesy constrains
 721 ice age terminal deglaciation: The global ICE-6G-C (VM5a) model. *Jour-*
 722 *nal of Geophysical Research - Solid Earth*, *120*, 450–487. doi: 10.1002/
 723 2014JB011176
- 724 Petoukhov, V., Ganopolski, A., Brovkin, V., Claussen, M., Eliseev, A., Kubatzki, C.,
 725 & Rahmstorf, S. (2000). CLIMBER-2: a climate system model of intermediate
 726 complexity. Part I: model description and performance for present climate.
 727 *Climate dynamics*, *16*(1), 1–17. doi: 10.1007/PL00007919
- 728 Roche, D. M., Crosta, X., & Renssen, H. (2012). Evaluating Southern Ocean
 729 sea-ice for the Last Glacial Maximum and pre-industrial climates: PMIP-
 730 2 models and data evidence. *Quat. Sci. Rev.*, *56*, 99–106. doi: 10.1016/
 731 j.quascirev.2012.09.020
- 732 Roche, D. M., Dokken, T. M., Goosse, H., Renssen, H., & Weber, S. L. (2007).
 733 Climate of the Last Glacial Maximum: sensitivity studies and model-data com-
 734 parison with the LOVECLIM coupled model. *Clim. Past*, *3*(2), 205–224. doi:
 735 10.5194/cpd-2-1105-2006
- 736 Schmittner, A., & Galbraith, E. D. (2008). Glacial greenhouse-gas fluctuations con-
 737 trolled by ocean circulation changes. *Nature*. doi: 10.1038/nature07531
- 738 Sigman, D. M., & Boyle, E. A. (2000). Glacial/interglacial variations in atmospheric
 739 carbon dioxide. *Nature*, *407*, 859–869. doi: 10.1038/35038000

- 740 Sigman, D. M., Hain, M. P., & Haug, G. H. (2010). The polar ocean and glacial
741 cycles in atmospheric CO₂ concentration. *Nature*, *466*, 47–55. doi: 10.1038/
742 nature09149
- 743 Six, K. D., & Maier-Reimer, E. (1996). Effects of plankton dynamics on seasonal
744 carbon fluxes in an ocean general circulation model. *Global Biogeochem. Cy.*,
745 *10*, 559–583.
- 746 Skinner, L. C. (2009). Glacial-interglacial atmospheric CO₂ change: a possible
747 standing volume effect on deep-ocean carbon sequestration. *Clim. Past*, *5*,
748 537–550. doi: 10.5194/cp-5-537-2009
- 749 Stephens, B. B., & Keeling, R. F. (2000). The influence of Antarctic sea ice on
750 glacial-interglacial CO₂ variations. *Nature*, *404*, 171–174.
- 751 Tagliabue, A., Aumont, O., & Bopp, L. (2014). The impact of different external
752 sources of iron on the global carbon cycle. *Geophys. Res. Lett.*, *41*, 920–926.
753 doi: 10.1002/2013GL059059
- 754 Tagliabue, A., Bopp, L., Roche, D. M., Bouttes, N., Dutay, J.-C., Alkama, R., . . .
755 Paillard, D. (2009). Quantifying the roles of ocean circulation and biogeochem-
756 istry in governing ocean carbon-13 and atmospheric carbon dioxide at the last
757 glacial maximum. *Clim. Past*, *5*, 695–706. doi: 10.5194/cp-5-695-2009
- 758 Watson, A. J., Vallis, G. K., & Nikurashin, M. (2015). Southern Ocean buoyancy
759 forcing of ocean ventilation and glacial atmospheric CO₂. *Nature geoscience*.
760 doi: 10.1038/NCEO2538
- 761 Yamamoto, A., Abe-Ouchi, A., Ohgaito, R., Ito, A., & Akira Oka, A. (2019). Glacial
762 CO₂ decrease and deep-water deoxygenation by iron fertilization from glacio-
763 genic dust. *Clim. Past*, *15*(3), 981–996. doi: 10.5194/cp-15-981-2019
- 764 Yamamoto, A., Abe-Ouchi, A., & Yamanaka, Y. (2018). Long-term response of
765 oceanic carbon uptake to global warming via physical and biological pumps.
766 *Biogeosciences*, *15*, 4163–4180. doi: 10.5194/bg-15-4163-2018